

Electronic Supplementary Information Section

A single emitting layer white OLED based on exciplex interface emission

Enrico Angioni, Marian Chapran, Khrystyna Ivaniuk, Nataliya Kostiv, Vladyslav Cherpak, Pavlo Stakhira, Algirdas Lazauskas, Sigitas Tamulevičius, Dmytro Volyniuk, Neil J. Findlay, Tell Tuttle, Juozas V. Grazulevicius, * Peter J. Skabara**

General Experimental

All reactions were performed using vacuum Schlenk lines, in an inert atmosphere of nitrogen. Dry solvents were obtained from a solvent purification system (SPS 400 from Innovative Technologies) using alumina as the drying agent. The compounds 4-iodo-3-hydroxybenzoic acid,¹ methyl 4-iodo-3-hydroxybenzoate,¹ methyl 4-iodo-3-methoxybenzoate (**2**)¹ were synthesised and analysed using literature procedures. All the other reagents were purchased from Sigma Aldrich or Alfa Aesar and used without further purifications. ¹H and ¹³C NMR spectra were recorded on a Bruker Avance DPX400 apparatus at 400.1 and 100.6 MHz. Chemical shifts are given in ppm; all *J* values are in Hz. MS LDI-TOF spectra were run on a Shimadzu Axima-CFR spectrometer (mass range 1-150000 Da). The high resolution mass measurements were performed on the Thermo Scientific LTQ ORBITRAP XL instrument, using the nano-electrospray ionisation (nano-ESI) technique. Thermogravimetric analysis (TGA) was performed using a Perkin-Elmer Thermogravimetric Analyser TGA7 under a constant flow of argon. Melting points were taken using a TA instruments DSC QC1000 Differential Scanning Calorimeter. Cyclic voltammetry (CV) measurements were performed on a CH Instruments 660A electrochemical workstation with *i*R compensation using anhydrous dichloromethane as the solvent. The electrodes were glassy carbon, platinum wire and silver wire as the working, counter and reference electrodes, respectively. All solutions were degassed (Ar) and contained the substrate in concentrations of *ca.* 10⁻⁴ M, together with n-Bu₄NPF₆ (0.1M) as the supporting electrolyte. All measurements are referenced against the E_{1/2} of the F_c/F_c⁺ redox couple. Absorption spectra were recorded on a Shimadzu UV 2700 instrument. Photoluminescence measurements were recorded using a Perkin-Elmer LS 50 B fluorescence spectrometer in a quartz cuvette (path length 10 mm). Absolute photoluminescence quantum yield measurements were measured according to the de Mello² method by using a calibrated integrating sphere attached to an USB 2000 spectrometer and Gooch & Housego spectrometer. Excitation light was chosen from a Quartz Tungsten

Halogen lamp by using a Gooch & Housego spectrometer and the emission light was collected by Ocean optics USB 2000 spectrometer. Measurements were performed in air. The ionisation potential of **1** was measured by the electron photoemission method in air.³ The samples were fabricated by means of vacuum deposition of **1** onto an indium tin oxide (ITO) coated glass substrate. The experimental setup consists of the deep-UV deuterium light source ASBN-D130-CM, the CM110 1/8m monochromator, and the 6517B Keithley electrometer. Characteristics of the current density–voltage and luminance–voltage dependences were measured with a semiconductor parameter analyser (HP 4145A) using it in air without passivation immediately after fabrication of the device. The measurement of brightness was performed using a calibrated photodiode.⁴ Calibration of the photodetector was carried out using a radiometer RTN 20 (accuracy $\pm 2\%$). The photodiode was placed in front of the OLED in a dark room and the calibration was performed according to the method described earlier.⁵ The external quantum efficiency (EQE) values were determined using the equations given in reference 6. The OLED electroluminescence and photoluminescence (PL) spectra of the solid films were recorded with an Ocean Optics USB2000 spectrometer. For the spectral studies the single layers of **1** as well as the **1:TPD** composite layer were prepared by thermovacuum deposition at 10^{-6} Torr onto clean quartz substrates or spin coating *ca.* 2M solutions of **1** as well as **1/TPD** onto clean quartz substrates. Luminescence spectra and luminescence decay curves of the layers were recorded with an Edinburgh Instruments FLS980 spectrometer at 77 K and room temperature using a low repetition rate μ F920H Xenon Flashlamp as the excitation source. The emission was measured twice: immediately after excitation and with a delay after the pulse was turned off (the delay time was set to be *ca.* 30 μ s). Chromaticity coordinates (CIE 1931) and correlated colour temperatures (CCT) are calculated from the response-corrected spectra. X-ray diffraction measurements at grazing incidence (XRDGI) were performed using a D8 Discover diffractometer (Bruker) with Cu K_{α} ($\lambda = 1.54 \text{ \AA}$) X-ray source. Parallel beam geometry with a 60 mm Göbel mirror (X-ray mirror on a high precision parabolic surface) was used. This configuration enables transforming the divergent incident X-ray beam from a line focus of the X-ray tube into a parallel beam that is free of K_{β} radiation. The primary side also had a Soller slit with an axial divergence of 2.5° . The secondary side had a LYNXEYE (0D mode) detector with an opening angle of 1.275° and slit opening of 9.5 mm. The sample stage was a Centric Eulerian cradle mounted to a horizontal D8 Discover with a vacuum chuck (sample holder) fixed on the top of the stage. X-ray generator voltage and current was 40.0 kV and 40 mA, respectively. XRDGI scans were performed in the range of $5.0\text{-}135.0^{\circ}$ with a step size of 0.066° , time per step of 0.2 s

and auto-repeat function enabled. The resultant diffractograms were processed with the software DIFFRAC.EVA. AFM experiments were carried out in air at room temperature using a NanoWizardIII atomic force microscope (JPK Instruments), while data were analysed using SurfaceXplorer and JPKSPM Data Processing software. AFM images were collected using a V-shaped silicon cantilever (spring constant of 3 N/m, tip curvature radius of 10.0 nm and the cone angle of 20°) operating in contact mode. The space-charge-limited current (SCLC) measurements were adopted for the estimation of charge drift mobility of **1**. Hole-only and electron-only devices were fabricated as described in the paper. The current density vs. voltage characteristics of the hole-only and electron-only devices were recorded and fitted using the Mott-Gurney law:⁷

$$J_{SCLC} = \mu_0 \frac{9V^2}{8d^3} \epsilon \epsilon_0 (0.891\gamma\sqrt{V/d}) \quad (1)$$

J_{SCLC} is the steady-state current density; μ_0 is the zero field mobility; V is applied voltage; d is the film thickness, ϵ is the permittivity of the film (~ 3); ϵ_0 is the vacuum permittivity and γ is the field dependence parameter. The ITO-coated glass substrates had a sheet resistance of 15 Ω/sq and the organic layers were deposited in top of it at a rate $< 0.1 \text{ \AA}/\text{s}$, using a MB EcoVap4G vacuum deposition system build in a Kurt J. Lesker glove box. The sample area was of 6 mm^2 . The charge drift mobility of **1** was estimated as previously described from J. C. Blakesley *et al.*⁸ All the theoretic calculations were performed with the software package Gaussian09 (Revision A.02).⁹

Synthesis of dimethyl 4,4'-(benzo[c][1,2,5]thiadiazole-4,7-diyl)bis(3-methoxybenzoate) (**1**)

4,7-Bis(4,4,5,5-tetramethyl-1,3,2-dioxaborolan-2-yl)benzo[c][1,2,5]thiadiazole (100 mg, 0.258 mmol), potassium phosphate (109 mg, 0.515 mmol), [1,1'-bis(diphenylphosphino)ferrocene]-dichloropalladium(II) dichloromethane adduct (21 mg, 0.026 mmol) and methyl 4-iodo-3-methoxybenzoate (226 mg, 0.773 mmol) were charged under nitrogen in a two-neck round-bottom flask. Degassed water (1 mL) and dimethylformamide (9 mL) were added and the mixture was stirred at 60°C for 18 hours. After this time the mixture was diluted with brine (50 mL) and extracted with dichloromethane (3 x 50 mL). The recombined organic layers were washed with brine (2 x 50 mL), water (3 x 50 mL), dried over MgSO_4 and concentrated under reduced pressure to

afford a dark yellow solid. Purification on silica gel, eluting dichloromethane to wash off the impurities and then chloroform afforded a dark yellow powder. The title compound (**1**) was obtained after recrystallisation from hot acetone as a bright yellow powder (69 mg, 58%). TGA: 5% mass loss at 311 °C; $T_m = 227$ °C, $T_c = 147$ °C; ^1H NMR (400.1 MHz, CDCl_3 , δ) 7.81 (dd, $J = 7.8, 1.5$ Hz, 2H, Ar H), 7.77 (d, $J = 1.5$ Hz, 2H, Ar H), 7.76 (s, 2H, Ar H), 7.65 (d, $J = 7.8$ Hz, 2H, ArH), 3.97 (s, 6H, COOCH_3), 3.88 (s, 6H, OCH_3); ^{13}C NMR (100.6 MHz, CDCl_3 , δ) 166.9, 157.2, 154.1, 131.9, 131.5, 131.2, 130.5, 129.9, 122.1, 112.4, 56.1, 52.4; MALDI (m/z (%)) 464.15 (100), 465.12 (75), 466.14 (30); HRMS (LSI-TOF) m/z [$\text{M} + \text{H}$] $^+$ calcd for $\text{C}_{24}\text{H}_{21}\text{N}_2\text{O}_6\text{S}$ 465.1115, found 465.1117. Melting Point: 230-232 °C.

Table S1. Energies, wavelengths, oscillator strengths, symmetry and orbital assignments of the first 20 singlet vertical electronic transitions for **1** (vacuum) calculated at the PBE0/6-311G(d,p) level of theory.

| Energy (eV) | Wavelength h (nm) | Oscillator Strength | Symmetry | Major contributions |
|-------------|-------------------|---------------------|----------|--|
| 2.99 | 415.0 | 0.4026 | Singlet | HOMO->LUMO (98%) |
| 3.49 | 355.3 | 0.0074 | Singlet | H-1->LUMO (99%) |
| 3.74 | 331.3 | 0.0267 | Singlet | H-2->LUMO (96%) |
| 3.98 | 311.2 | 0.6020 | Singlet | HOMO->L+1 (95%) |
| 4.12 | 300.9 | 0.0058 | Singlet | H-3->LUMO (74%), HOMO->L+2 (13%) |
| 4.33 | 286.1 | 0.0636 | Singlet | H-4->LUMO (25%), HOMO->L+2 (63%) |
| 4.48 | 276.7 | 0.0509 | Singlet | H-4->LUMO (52%), H-1->L+1 (12%), HOMO->L+2 (10%) |
| 4.55 | 272.4 | 0.0443 | Singlet | H-1->L+1 (64%), HOMO->L+2 (10%) |
| 4.62 | 268.6 | 0.0248 | Singlet | H-2->L+1 (50%), H-1->L+2 (31%) |
| 4.73 | 262.2 | 0.0178 | Singlet | H-5->LUMO (89%) |
| 4.74 | 261.4 | 0.0002 | Singlet | H-8->LUMO (43%), H-6->LUMO (32%) |
| 4.78 | 259.3 | 0.0002 | Singlet | H-7->LUMO (63%), H-7->L+1 (14%), H-6->L+2 (17%) |
| 4.81 | 257.9 | 0.0000 | Singlet | H-8->LUMO (33%), H-7->L+2 (13%), H-6->LUMO (31%), H-6->L+1 (12%) |
| 4.98 | 249.1 | 0.0460 | Singlet | H-2->L+1 (36%), H-1->L+2 (61%) |
| 5.00 | 248.0 | 0.0001 | Singlet | H-3->L+1 (11%), H-2->L+2 (59%), H-1->L+1 (17%) |
| 5.05 | 245.8 | 0.0027 | Singlet | H-11->LUMO (79%) |
| 5.14 | 241.4 | 0.0162 | Singlet | H-4->L+1 (10%), H-3->L+1 (65%), H-2->L+2 (17%) |
| 5.22 | 237.6 | 0.0002 | Singlet | H-7->L+2 (25%), H-6->LUMO (36%), H-6->L+1 (32%) |
| 5.32 | 233.1 | 0.0057 | Singlet | H-7->LUMO (33%), H-7->L+1 (25%), H-6->L+2 (22%) |
| 5.33 | 232.5 | 0.0630 | Singlet | H-3->L+2 (17%), HOMO->L+4 (58%) |

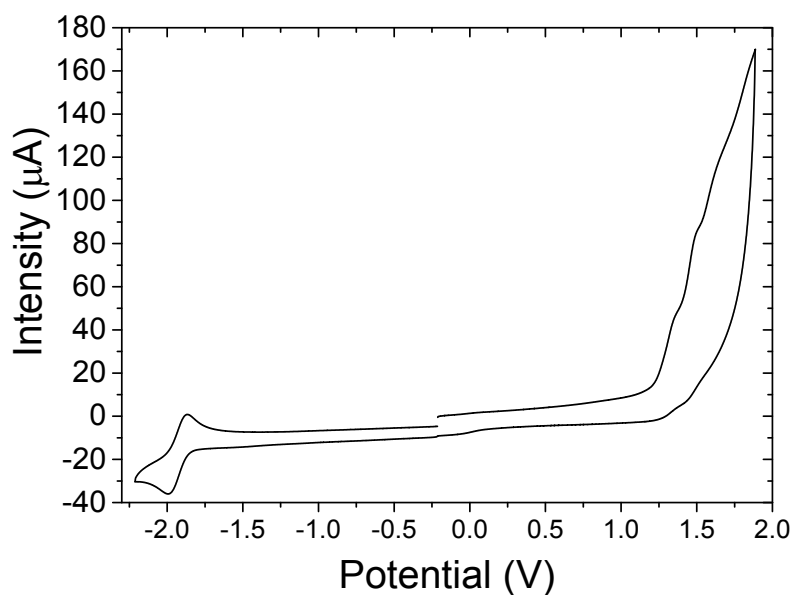


Figure S1. Cyclic voltammogram of **1** ($1 \cdot 10^{-4}$ M solution). Measurements performed using a glassy carbon working electrode, Ag/AgCl reference electrode and platinum wire counter electrode. The supporting electrolyte was 0.1M tetrabutylammonium hexafluorophosphate in dichloromethane. Scan rate of 0.1 Vs^{-1} . All the waves were referenced to ferrocene.

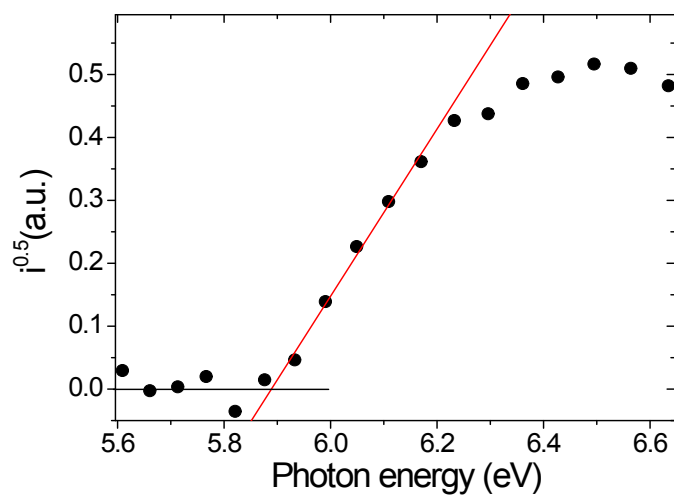


Figure S2. Photoelectron emission spectrum of a thin layer of **1**.

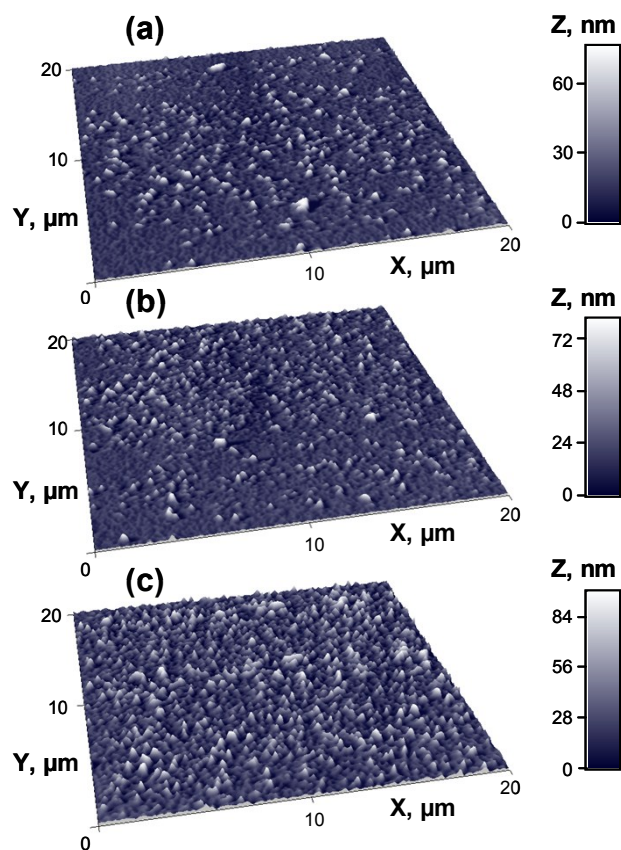


Figure S3. AFM 3D topographical images with normalized Z axis in nm of thin films (30 nm) of **1** prepared by vacuum evaporation at different deposition rates on glass substrates: (a) $<0.1 \text{ \AA/s}$, (b) 1.5 \AA/s and (c) 10 \AA/s . The images were acquired in air using contact mode.

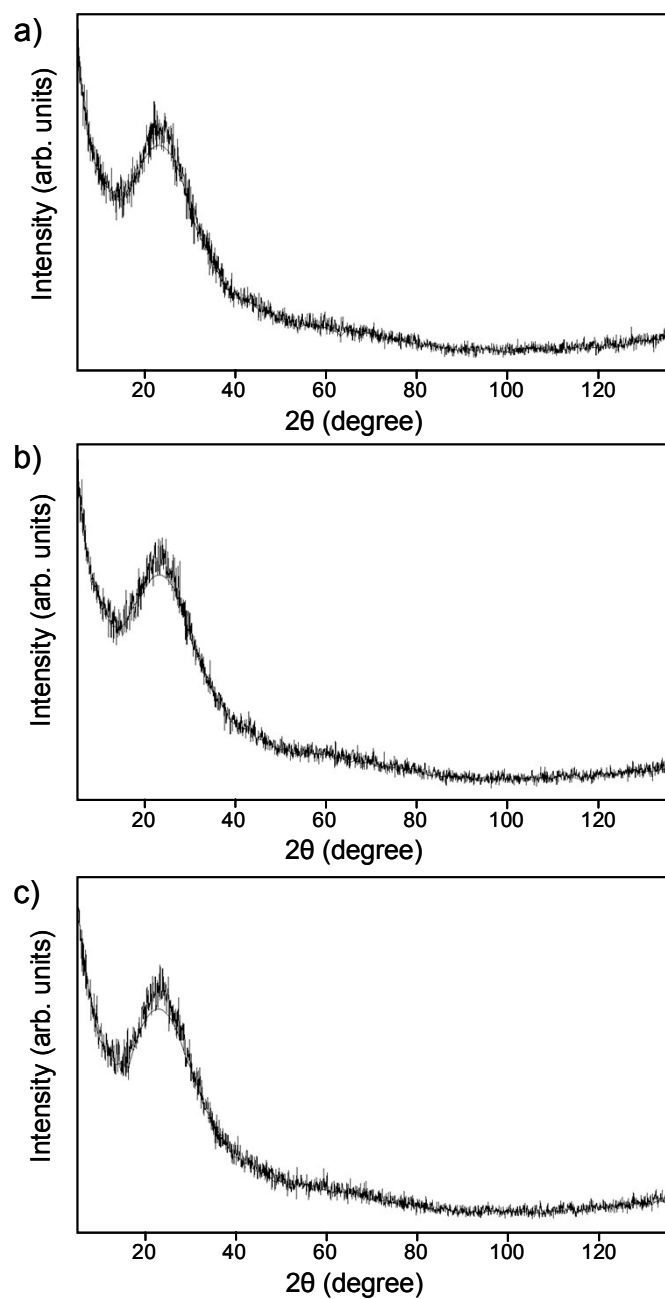


Figure S4. X-ray diffraction patterns a grazing incidence angle of 1.50° of thin films of **1** prepared by vacuum evaporation at different deposition rates on glass substrates: (a) $<0.1 \text{ \AA/s}$, (b) 1.5 \AA/s and (c) 10 \AA/s .

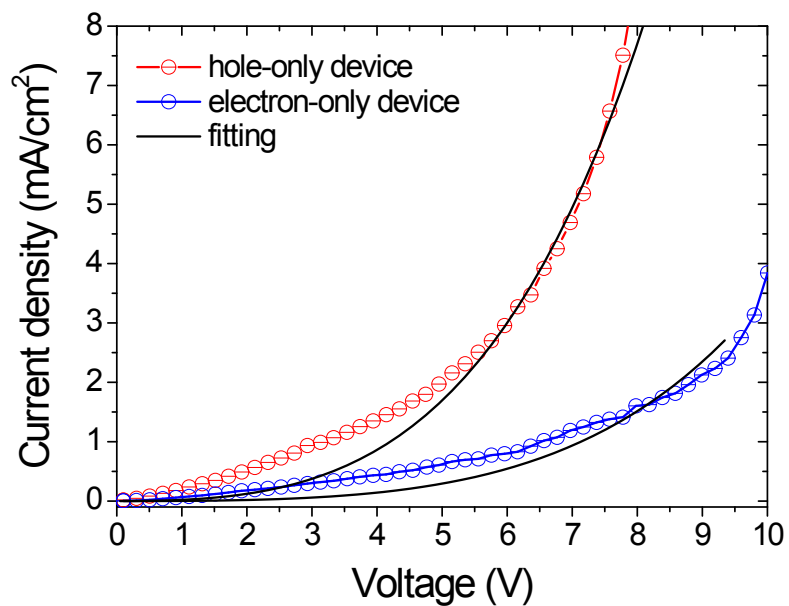


Figure S5 Current density-voltage characteristic curves and fittings of the hole only and electron only devices. The disagreement between the experimental and fit curves can be explained taking in account the existence of electron and hole traps in **1** due to its morphology.

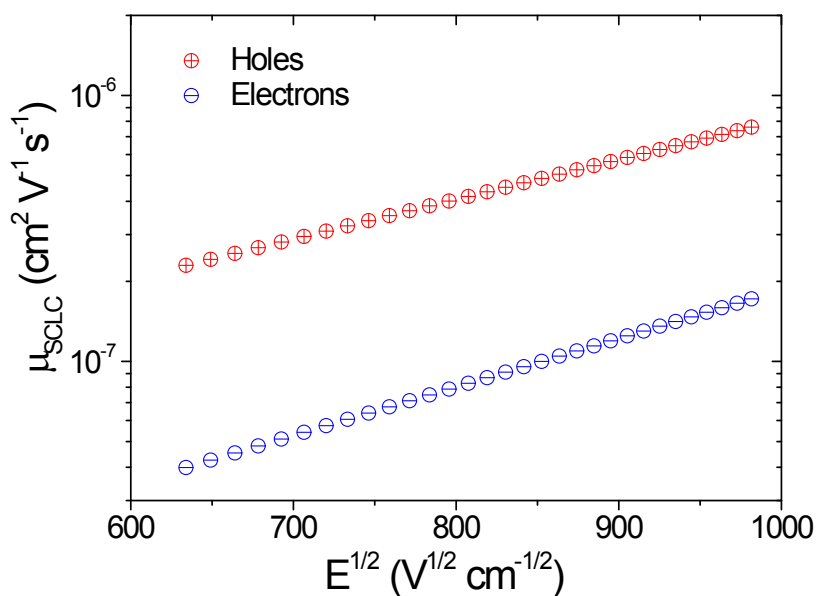


Figure S6 Hole and electron mobility of **1** at different square root of the applied electric field.

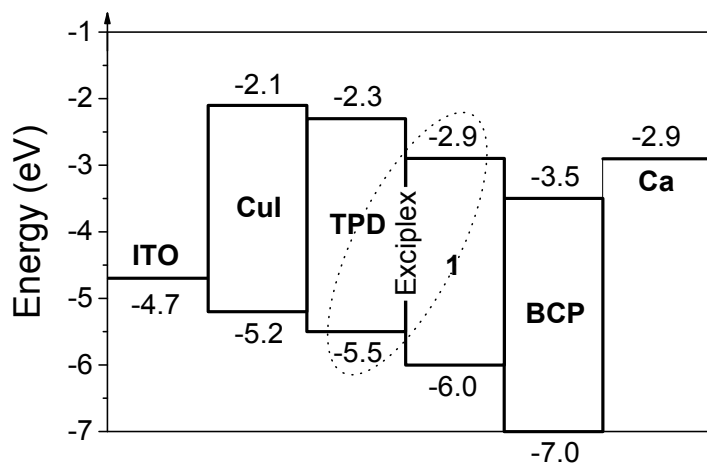


Figure S7. Energy-band diagram of the fabricated device. Aluminium was used on the cathode for the passivation of the calcium electrode, in order to investigate the properties of the device in ambient atmosphere at room temperature immediately after device fabrication.

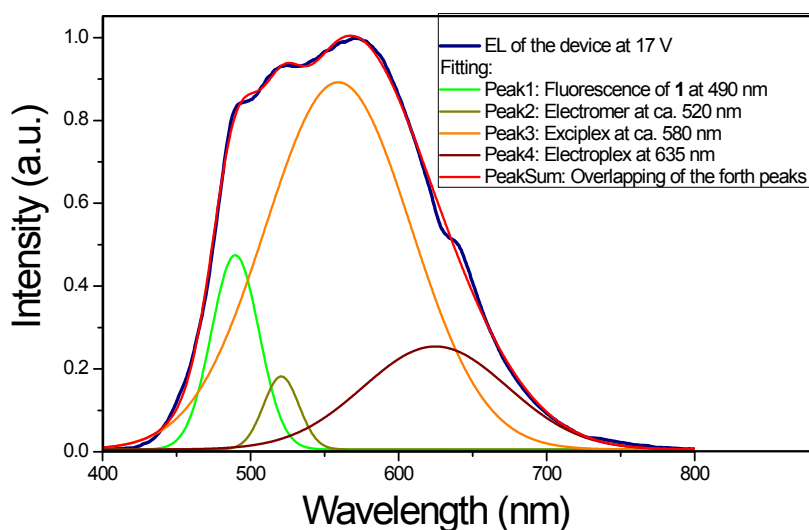


Figure S8. Fitting of the electroluminescence spectrum at 17 V of the OLED, providing the assignments of the different peaks.

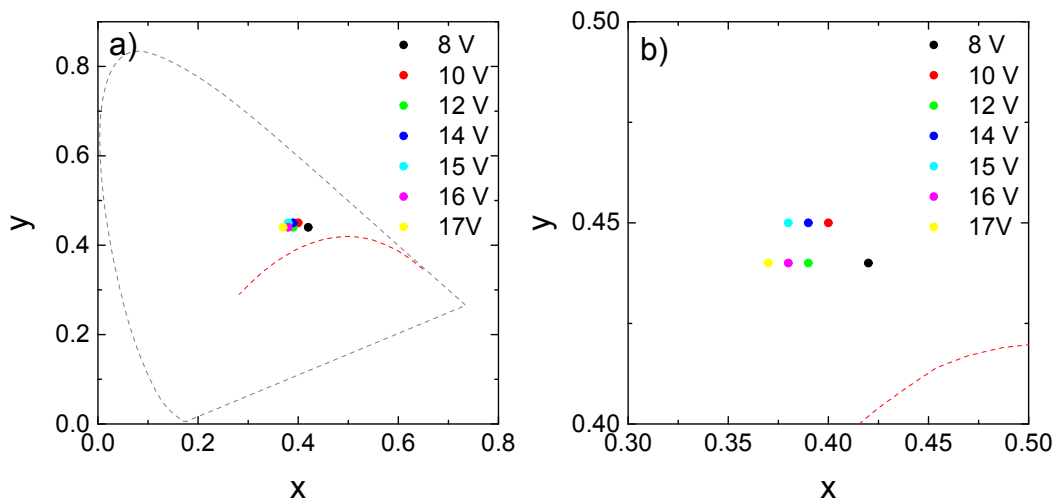


Figure S9 The different colour coordinates of the device under different applied voltages.

Table S2. The different colour coordinates of the device under different applied voltages.

| Applied voltage (V) | CIE 1931 coordinates |
|---------------------|----------------------|
| 8 | (0.42, 0.44) |
| 10 | (0.40, 0.45) |
| 12 | (0.39, 0.44) |
| 14 | (0.39, 0.45) |
| 15 | (0.38, 0.45) |
| 16 | (0.38, 0.44) |
| 17 | (0.37, 0.44) |

Table S3. Summary of the characteristics of the device.

| V_{on} at 1.4 Cd/m ² (V) | Max Brightness (cd/m ²) | Max current efficiency (cd/A) | Max power Efficiency (lm/W) | Max external Quantum efficiency (%) | CIE 1931 Coordinates (x, y) | Colour Temperature (K) |
|---|---|-------------------------------------|-----------------------------------|---|-----------------------------------|------------------------------|
| 5.8 | 5219 | 6.5 | 2.6 | 2.39 | (0.39, 0.44) | 4500 |

Table S4. Current efficiency, power efficiency and external quantum efficiency of the device at different current densities and brightness.

| Current density | Current efficiency (cd/A) | Power efficiency (lm/W) | External quantum efficiency (%) |
|------------------------|---------------------------|-------------------------|---------------------------------|
| 10 mA/cm ² | 6.23 | 1.96 | 2.3 |
| 100 mA/cm ² | 3.99 | 2.57 | 1.47 |
| Brightness | | | |
| 100 Cd/m ² | 6.55 | 0.96 | 2.42 |
| 1000 Cd/m ² | 5.31 | 1.54 | 1.96 |

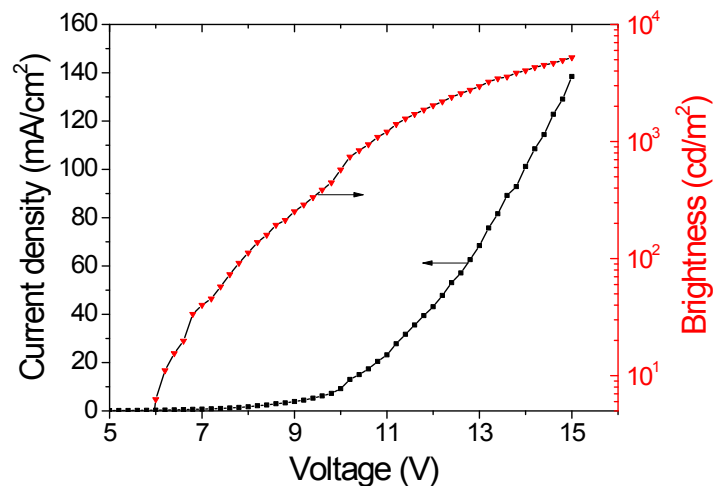


Figure S10. Current density–voltage and luminance–voltage characteristics of the device.

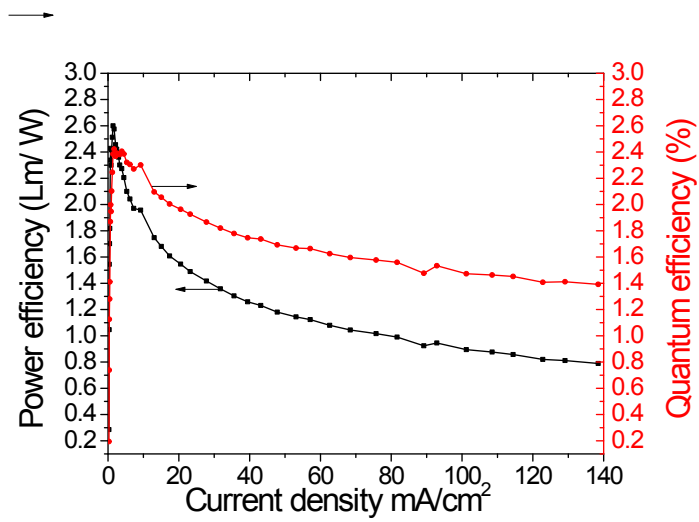


Figure S11. Power efficiency and external quantum efficiency of the device.

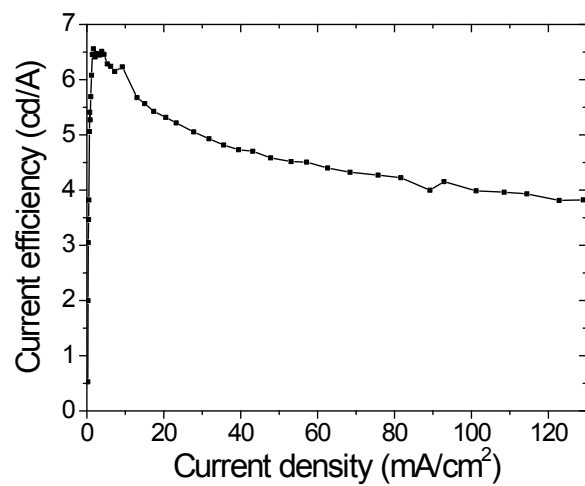


Figure S12. Current efficiency–current density characteristic of the device.

Table S5. Mean signed and mean square errors (MSiE and MSqE, eV) and maximal deviations (Max-Min, eV), obtained by comparing experimental and theoretical mean maximum absorption values of literature compound 4,7-dithiophenyl-benzothiadiazole (**3**).¹⁰ Using the TD-DFT method including the polarisable continuum model (PCM)¹¹ (dichloromethane) the vertical transitions were calculated for **3**, using the combination of five different functionals (B3LYP¹², wB97xD,¹³ CAM-B3LYP,¹⁴ M06-2X,¹⁵ PBE0)¹⁶ and three different basis sets (6-31G, 6-311G(d,p), 6-311+G(2d,p), DGDZVP). Six vertical absorptions were simulated at each level of theory and they were fitted with Gaussian curves (full width at half maximum (FWHM) = 0.37 eV) using the software GaussSum 3.0.¹⁷ The two maxima obtained with this procedure were compared with the experimental maxima absorption bands of **3**. The level of theory PBE0/6-311G(d,p) have shown the smallest mean signed and mean square errors (the smallest shift of the vertical absorptions calculated in comparison with the experimental data) and it was used for all further calculations.

| | B3LYP | | | | wB97X-D | | | |
|---------------|--------|-------------|---------------|--------|---------|-------------|---------------|--------|
| | 6-31G | 6-311G(d,p) | 6-311+G(2d,p) | DGDZVP | 6-31G | 6-311G(d,p) | 6-311+G(2d,p) | DGDZVP |
| MSiE | -0.323 | -0.281 | -0.319 | -0.397 | 0.463 | 0.475 | 0.436 | 0.436 |
| MSqE | 0.113 | 0.087 | 0.109 | 0.166 | 0.231 | 0.241 | 0.199 | 0.202 |
| Max(+) | -0.228 | -0.190 | -0.236 | -0.306 | 0.593 | 0.601 | 0.531 | 0.546 |
| Min(-) | -0.418 | -0.372 | -0.402 | -0.488 | 0.334 | 0.349 | 0.341 | 0.326 |

| | CAM-B3LYP | | | | M06-2X | | | |
|---------------|-----------|-------------|---------------|--------|--------|-------------|---------------|--------|
| | 6-31G | 6-311G(d,p) | 6-311+G(2d,p) | DGDZVP | 6-31G | 6-311G(d,p) | 6-311+G(2d,p) | DGDZVP |
| MSiE | 0.363 | 0.405 | 0.359 | 0.316 | 0.363 | 0.421 | 0.351 | 0.335 |
| MSqE | 0.155 | 0.182 | 0.139 | 0.117 | 0.160 | 0.197 | 0.134 | 0.130 |
| Max(+) | 0.515 | 0.539 | 0.461 | 0.446 | 0.531 | 0.562 | 0.453 | 0.469 |
| Min(-) | 0.210 | 0.272 | 0.256 | 0.186 | 0.194 | 0.279 | 0.248 | 0.202 |

| | PBE0 | | | |
|---------------|--------|-------------|---------------|--------|
| | 6-31G | 6-311G(d,p) | 6-311+G(2d,p) | DGDZVP |
| MSiE | -0.153 | -0.114 | -0.153 | -0.153 |
| MSqE | 0.037 | 0.025 | 0.032 | 0.034 |
| ax(+) | -0.035 | -0.004 | -0.058 | -0.050 |
| Min(-) | -0.271 | -0.224 | -0.248 | -0.255 |

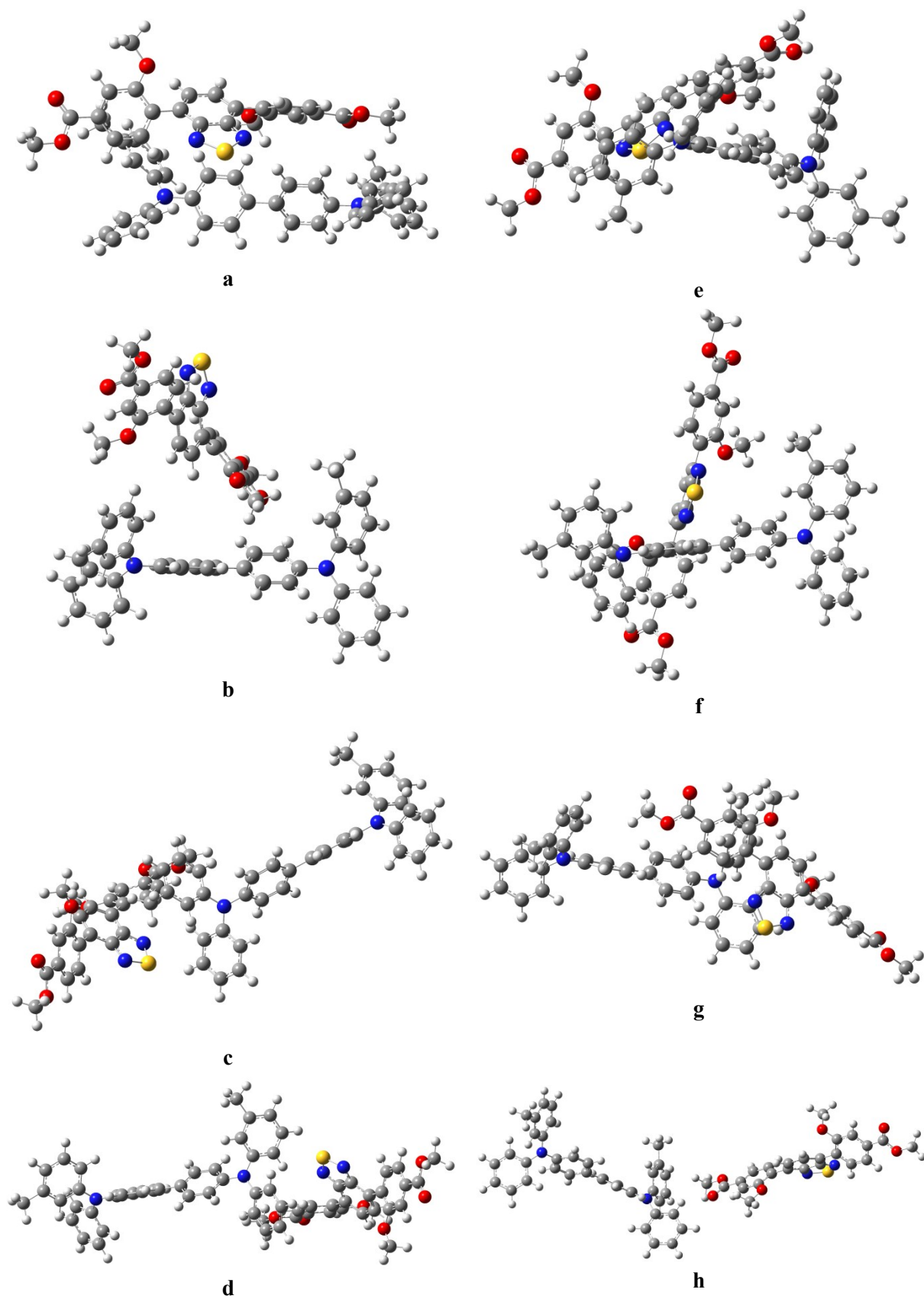


Figure S13. Optimised geometries for height different TPD:1 complexes (a-h), calculated at the PBE0/6-311G(d,p) level of theory.

Table S6. Relative total energies for height different **TPD:1** complexes (**a-h**), calculated at the PBE0/6-311G(d,p) level of theory.

| Complex | Relative total energy (kcal/mol) |
|---------|-------------------------------------|
| a | 0.00 |
| b | 2.42 |
| c | 2.97 |
| d | 3.40 |
| e | 1.30 |
| f | 3.95 |
| g | 1.92 |
| h | 3.29 |

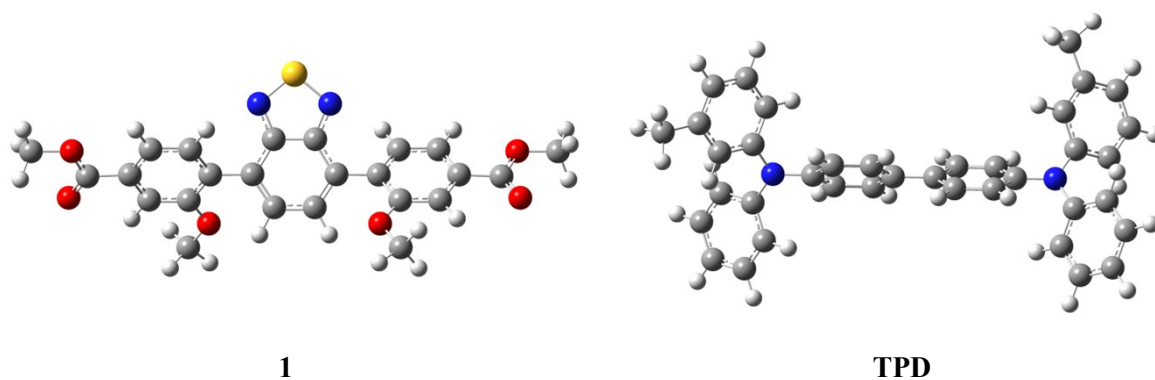


Figure S14. Optimised geometries of **1** and **TPD** calculated at the PBE0/6-311G(d,p) level of theory.

Table S7. Energies, wavelengths, oscillator strengths, symmetry and orbital assignments of the first 20 singlet vertical electronic transitions for **TPD** (vacuum) calculated at the PBE0/6-311G(d,p) level of theory.

| Energy (eV) | Wavelength (nm) | Oscillator Strength | Symmetry | Major contributions |
|-------------|-----------------|---------------------|----------|--|
| 3.48 | 356.0 | 1.0686 | Singlet | HOMO->LUMO (96%) |
| 3.78 | 328.0 | 0.0097 | Singlet | H-1->L+2 (14%), HOMO->L+1 (83%) |
| 3.84 | 323.3 | 0.0191 | Singlet | H-1->L+1 (21%), HOMO->L+2 (75%) |
| 3.95 | 313.8 | 0.0005 | Singlet | H-1->LUMO (95%) |
| 4.03 | 307.5 | 0.1855 | Singlet | H-1->L+3 (17%), HOMO->L+3 (78%) |
| 4.05 | 306.2 | 0.1792 | Singlet | H-1->L+4 (16%), HOMO->L+4 (80%) |
| 4.36 | 284.5 | 0.0661 | Singlet | H-1->L+2 (27%), HOMO->L+6 (56%) |
| 4.42 | 280.7 | 0.0005 | Singlet | H-1->L+1 (72%), HOMO->L+2 (19%) |
| 4.46 | 277.8 | 0.0009 | Singlet | HOMO->L+5 (52%), HOMO->L+8 (13%) |
| 4.48 | 277.0 | 0.0182 | Singlet | H-1->L+6 (15%), HOMO->L+7 (43%), HOMO->L+8 (11%), HOMO->L+9 (10%) |
| 4.51 | 275.1 | 0.0366 | Singlet | H-1->L+8 (13%), HOMO->L+7 (21%), HOMO->L+9 (42%) |
| 4.53 | 274.0 | 0.0041 | Singlet | H-1->L+2 (49%), HOMO->L+1 (11%), HOMO->L+6 (23%) |
| 4.59 | 270.3 | 0.0002 | Singlet | HOMO->L+5 (35%), HOMO->L+8 (43%) |
| 4.64 | 267.5 | 0.0403 | Singlet | H-1->L+3 (79%), HOMO->L+3 (18%) |
| 4.65 | 266.5 | 0.0387 | Singlet | H-1->L+4 (81%), HOMO->L+4 (17%) |
| 4.67 | 265.7 | 0.0262 | Singlet | H-1->L+5 (83%) |
| 4.69 | 264.4 | 0.0014 | Singlet | H-1->L+6 (74%), HOMO->L+9 (11%) |
| 4.70 | 263.6 | 0.0058 | Singlet | H-1->L+7 (31%), H-1->L+9 (43%), HOMO->L+6 (13%) |
| 4.80 | 258.2 | 0.0201 | Singlet | H-2->LUMO (16%), H-1->L+8 (38%), HOMO->L+7 (11%), HOMO->L+10 (13%) |
| 4.85 | 255.8 | 0.0001 | Singlet | H-1->L+7 (39%), H-1->L+9 (20%), HOMO->L+8 (22%) |

Table S8. Energies, wavelengths, oscillator strengths, symmetry and orbital assignments of the first 20 singlet vertical electronic transitions for the complex **TPD:1** (vacuum) calculated at the PBE0/6-311G(d,p) level of theory. It is assumed that emission can be generated from all the excited state energy levels.

| Energy (eV) | Wavelength (nm) | Oscillator Strength | Symmetry | Major contributions |
|-------------|-----------------|---------------------|----------|---|
| 2.06 | 600.7 | 0.0001 | Singlet | HOMO->LUMO (95%) |
| 2.44 | 508.7 | 0.0000 | Singlet | H-1->LUMO (94%) |
| 2.99 | 414.0 | 0.3039 | Singlet | H-2->LUMO (98%) |
| 3.09 | 401.7 | 0.0010 | Singlet | HOMO->L+1 (95%) |
| 3.33 | 372.9 | 0.0020 | Singlet | H-1->L+1 (30%), HOMO->L+2 (67%) |
| 3.49 | 355.1 | 0.0199 | Singlet | H-4->LUMO (48%), H-3->LUMO (48%) |
| 3.51 | 353.3 | 0.0006 | Singlet | H-1->L+1 (65%), HOMO->L+2 (25%) |
| 3.54 | 350.3 | 0.7465 | Singlet | HOMO->L+3 (93%) |
| 3.70 | 335.2 | 0.0080 | Singlet | H-5->LUMO (10%), H-4->LUMO (34%), H-3->LUMO (34%) |
| 3.74 | 331.8 | 0.0142 | Singlet | H-7->LUMO (36%), H-1->L+2 (52%) |
| 3.74 | 331.5 | 0.0215 | Singlet | H-7->LUMO (40%), H-1->L+2 (30%) |
| 3.75 | 330.6 | 0.0042 | Singlet | H-6->LUMO (23%), H-5->LUMO (45%), HOMO->L+4 (12%) |
| 3.78 | 328.4 | 0.0123 | Singlet | H-1->L+4 (18%), HOMO->L+4 (53%) |
| 3.81 | 325.4 | 0.0265 | Singlet | H-1->L+5 (13%), HOMO->L+5 (74%) |
| 3.82 | 324.8 | 0.0061 | Singlet | H-1->L+3 (83%) |
| 3.83 | 324.1 | 0.0016 | Singlet | H-9->LUMO (26%), H-6->LUMO (28%), H-5->LUMO (24%) |
| 3.86 | 321.0 | 0.5182 | Singlet | H-2->L+1 (87%) |
| 3.90 | 318.1 | 0.0003 | Singlet | H-8->LUMO (80%) |
| 3.94 | 314.9 | 0.0006 | Singlet | H-9->LUMO (51%), H-6->LUMO (28%) |
| 3.96 | 313.2 | 0.1328 | Singlet | H-1->L+6 (23%), HOMO->L+6 (66%) |

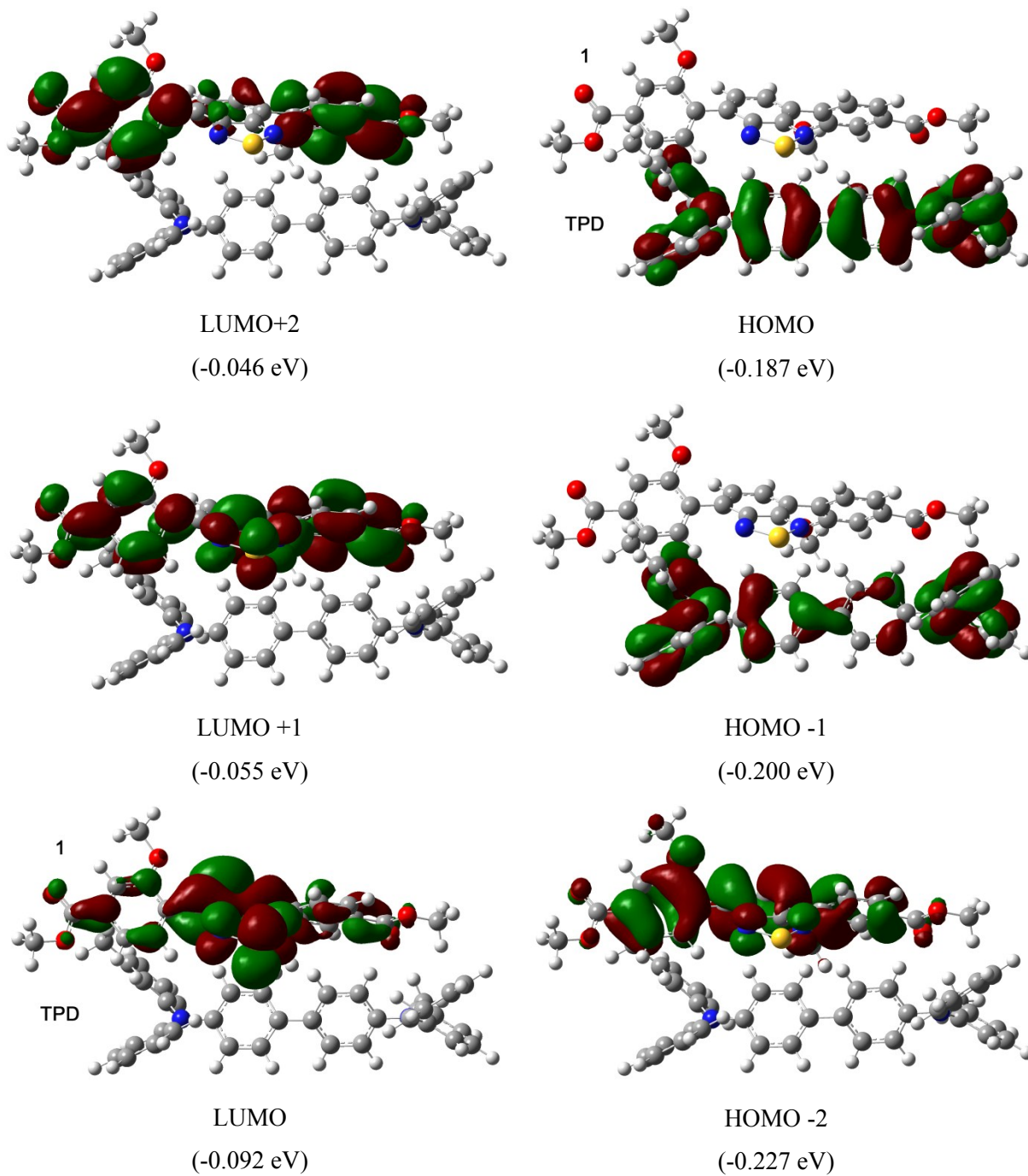


Figure S15. Molecular orbital graphical representations and energies (HOMO-2 to LUMO+2) of the **TPD:1** complex calculated at the PBE0/6-311G(d,p) level of theory (isosurface 0.02).

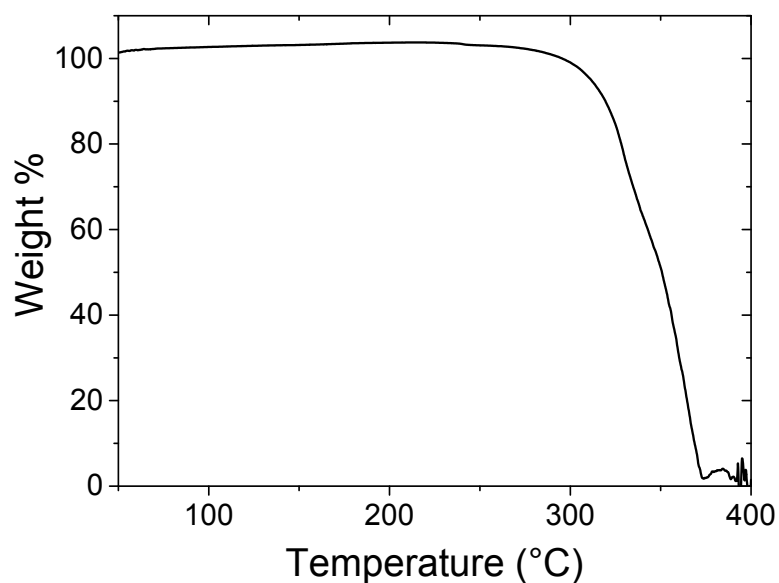


Figure S16. Thermogravimetric analyses of **1** in Argon (40-450°C). The small increment in the mass of the sample that is observed between 50 and 250°C is likely due to the Archimede's effect. When the object is under a current of fluid (nitrogen), the fluid tends to force the object upwards. When the analyser was tared the fluid (N₂) likely forced the sample upwards. In this way when the analysis starts, the density of the fluid was slightly decreased (by increasing the temperature) and consequently the hanged sample goes down. Then when these changes were recorded a mass increment is shown, produced by a small change in the density of the surrounding fluid. This effect is worse at higher heating rates.

D211974.1.fid — Person 7-16 — EA033_copy — @proton CDCl3 {C:\NMRdata} pjs 30

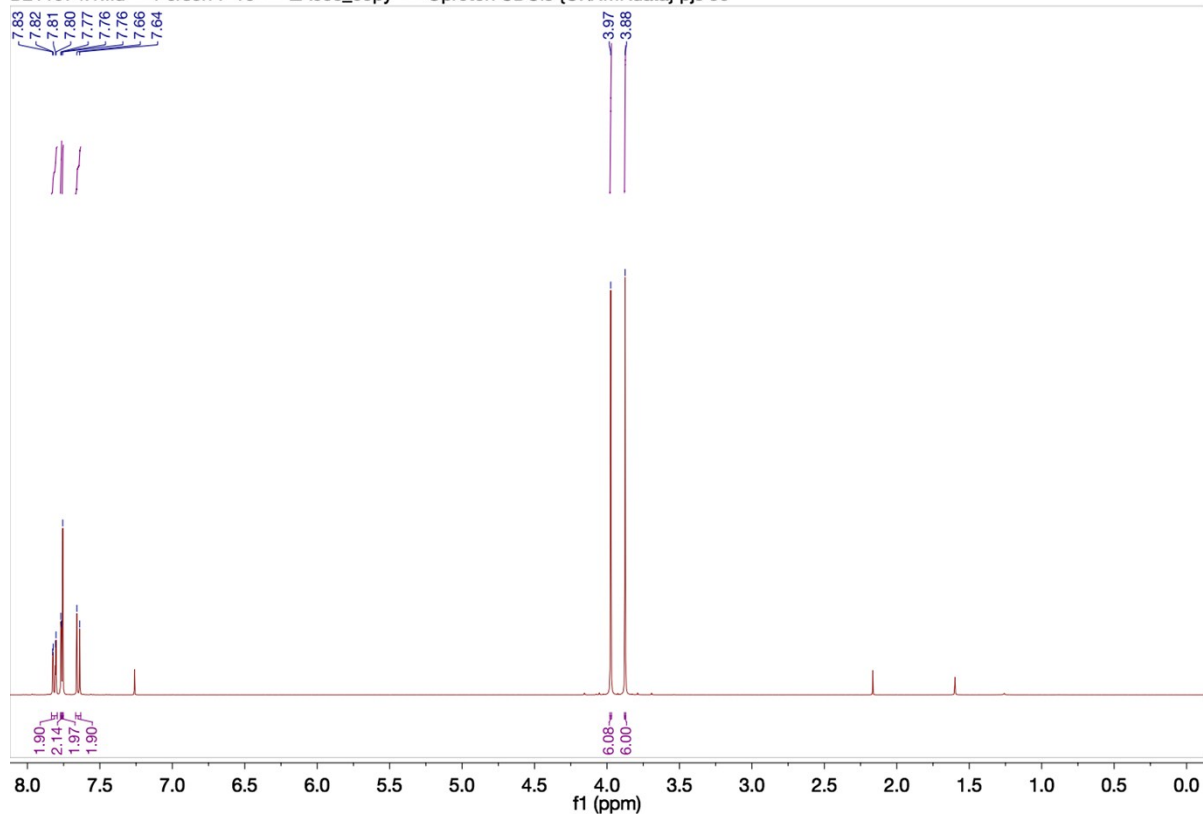


Figure S17. ¹H NMR spectrum of **1** recorded in deuterated chloroform.

D211974.2.fid — Person 7-16 — EA033_copy — ¹³C_@ CDCl3 {C:\NMRdata} pjs 30

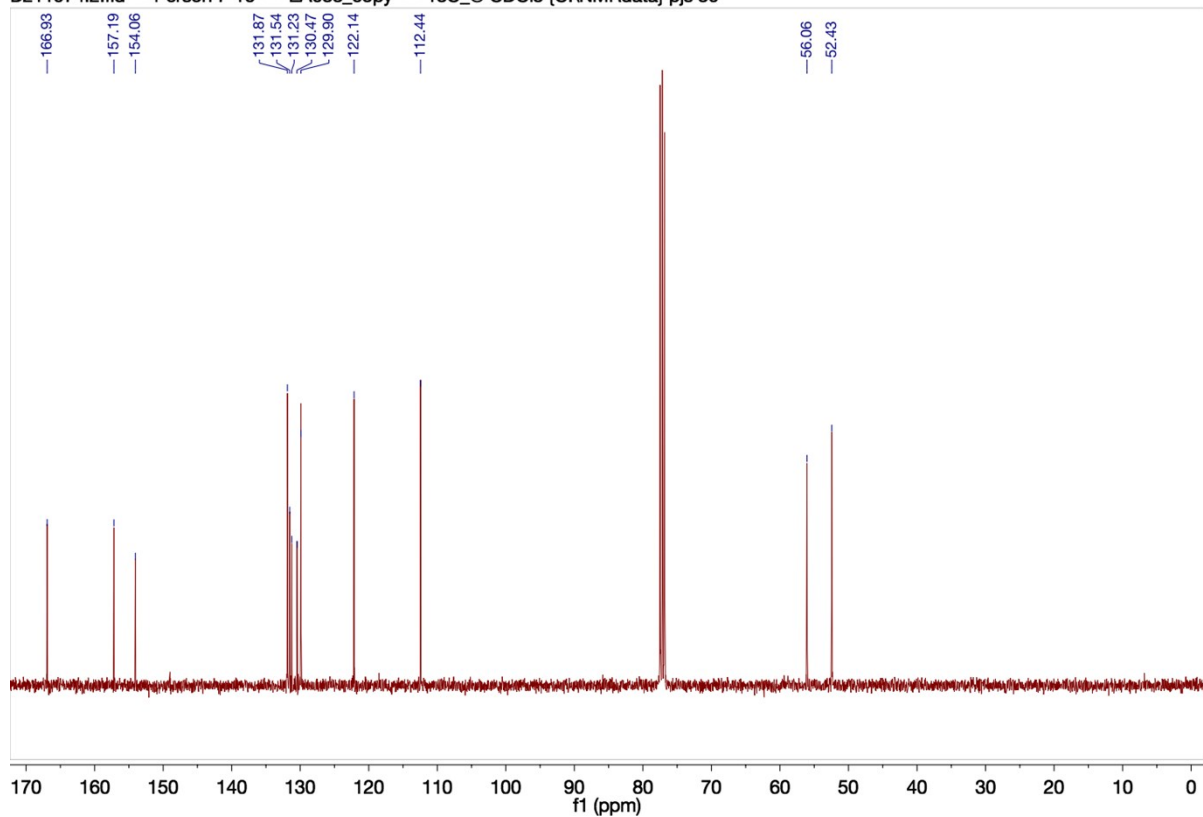


Figure S18. ¹³C NMR spectrum of **1** recorded in deuterated chloroform.

References

- 1 D. Rankine, A. Avellaneda, M. R. Hill, C. J. Doonan, C. J. Sumby, *Chem. Commun.*, **2012**, 48, 10328.
- 2 J. C. de Mello, H. F. Wittmann, R. H. Friend, *Adv. Mater.*, **1997**, 9, 230.
- 3 E. Miyamoto, Y. Yamaguchi, M. Yokoyama, *J. Imaging Sci. Technol.*, **1989**, 28, 364.
- 4 V. Cherpak, A. Gassmann, P. Stakhira, D. Volyniuk, J. V. Grazulevicius, A. Michaleviciute, A. Tomkeviciene, G. Barylo, H. von Seggern, *Org. Electron.*, **2014**, 15, 1396.
- 5 N. C. Greenham, R. H. Friend, D. D. C. Bradley, *Adv. Mater.*, **1994**, 6, 491.
- 6 M. A. F. Baldo, S. R.; Thompson, M. E. , *Organic Electroluminescence*, CRC Press, 2005.
- 7 N. F. Mott, R. W. Gurney, *Electronic Processes in Ionic Crystals*, Oxford, 1940.
- 8 J. C. Blakesley, F. A. Castro, W. Kylberg, G. F. A. Dibb, C. Arantes, R. Valaski, M. Cremona, J. S. Kim, J.-S. Kim, *Org. Electron.*, **2014**, 15, 1263.
- 9 M. J. Frisch, G. W. Trucks, H. B. Schlegel, G. E. Scuseria, M. A. Robb, J. R. Cheeseman, G. Scalmani, V. Barone, B. Mennucci, G. A. Petersson, H. Nakatsuji, M. Caricato, X. Li, H. P. Hratchian, A. F. Izmaylov, J. Bloino, G. Zheng, J. L. Sonnenberg, M. Hada, M. Ehara, K. Toyota, R. Fukuda, J. Hasegawa, M. Ishida, T. Nakajima, Y. Honda, O. Kitao, H. Nakai, T. Vreven, J. A. Montgomery Jr., J. E. Peralta, F. Ogliaro, M. J. Bearpark, J. Heyd, E. N. Brothers, K. N. Kudin, V. N. Staroverov, R. Kobayashi, J. Normand, K. Raghavachari, A. P. Rendell, J. C. Burant, S. S. Iyengar, J. Tomasi, M. Cossi, N. Rega, N. J. Millam, M. Klene, J. E. Knox, J. B. Cross, V. Bakken, C. Adamo, J. Jaramillo, R. Gomperts, R. E. Stratmann, O. Yazyev, A. J. Austin, R. Cammi, C. Pomelli, J. W. Ochterski, R. L. Martin, K. Morokuma, V. G. Zakrzewski, G. A. Voth, P. Salvador, J. J. Dannenberg, S. Dapprich, A. D. Daniels, Ö. Farkas, J. B. Foresman, J. V. Ortiz, J. Cioslowski, D. J. Fox, *Gaussian 09*, **2009**.
- 10 S.-i. Kato, T. Matsumoto, T. Ishi-i, T. Thiemann, M. Shigeiwa, H. Gorohmaru, S. Maeda, Y. Yamashita, S. Mataka, *Chem. Commun.*, **2004**, 2342.
- 11 S. Miertuš, E. Scrocco, J. Tomasi, *Chem. Phys.*, **1981**, 55, 117.
- 12 A. D. Becke, *J. Chem. Phys.*, **1993**, 98, 5648.
- 13 J.-D. Chai, M. Head-Gordon, *Phys. Chem. Chem. Phys.*, **2008**, 10, 6615.
- 14 T. Yanai, D. P. Tew, N. C. Handy, *Chem. Phys. Lett.*, **2004**, 393, 51.
- 15 Y. Zhao, D. Truhlar, *Theor. Chem. Acc.*, **2008**, 120, 215.
- 16 C. Adamo, V. Barone, *J. Chem. Phys.*, **1999**, 110, 6158.
- 17 N. M. O'Boyle, A. L. Tenderholt, K. M. Langner, *J. Comput. Chem.*, **2008**, 29, 839.